Frequency–dependence of power and efficiency for resonant inductive coupling and magnetoelectric wireless power transfer systems

IOP Publishing Smart Materials and Structures
Smart Mater. Struct. **31** (2022) 105026 (15pp) https://doi.org/10.1088/1361-665X/ac8bb6

Frequency–dependence of power and efficiency for resonant inductive coupling and magnetoelectric wireless power transfer systems

Erik Andersen, Shad Roundy and Binh Duc Truong*

Department of Mechanical Engineering, University of Utah, Salt Lake City, UT 84112, United States of America

E-mail: Binh.D.Truong@utah.edu

Received 22 June 2022, revised 4 August 2022
Accepted for publication 22 August 2022
Published 19 September 2022

Abstract

The frequency dependence of the maximum output power and efficiency of two wireless power transfer systems (WPTSs), resonant inductive coupling (RIC) and magnetoelectric (ME), are investigated. We find that in the weak–coupling regime, the power optimization and efficiency maximization problems are equivalent and yield the same optimal load and frequency. These properties apply to both topologies under consideration. Despite the apparent difference in the energy conversion mechanisms, the two structures result in similar explicit forms of maximum power delivered to the load, and so does the optimum transfer efficiency. We discuss the essential role of a figure of merit for each configuration and show how they affect the overall performance. For a weakly–coupled inductive WPTS, both the maximum transferred power and efficiency are positively proportional to drive frequency squared. In the case of a ME–based architecture, the dependence of power and efficiency on frequency is the consequence of the transducer geometry optimization problem, subject to a volume constraint. Under a constant mechanical quality factor condition, both quantities are linearly proportional to the operating frequency. While the focus of this paper is RIC and ME mechanisms, some of the findings are also valid for relevant inductive energy harvesting or magneto–mechano–electric WPTSs.

Keywords: power optimization, wireless power transfer, energy harvesting, frequency dependence

(Some figures may appear in colour only in the online journal)

1. Introduction

Wireless power transfer systems (WPTSs) actively transmit power from a source to a receiver, providing deterministic control over the generated power [1, 2]. This property has made wireless power transfer (WPT) a promising means to supply energy for low power electronics such as wireless sensors, especially for implantable devices where using traditional batteries raises many safety concerns [3–6]. Among methods based on electromagnetic fields, near–field resonant inductive coupling (RIC) is perhaps the most commonly used structure [7, 8]. In the last few years, WPTSs utilizing magnetoelectric (ME) effects have emerged as an attractive alternative, due to their excellent miniaturization potential, without compromising much of the power delivery capability [9–11]. In this work, we narrow our focus to these two methods.

* Author to whom any correspondence should be addressed.

Most WPTSs consider the link efficiency, defined by the ratio between the power delivered to the load and the power input to the transmitter, as the primary objective. However, the safety standards regulated by the Institute of Electrical and Electronics Engineers (IEEE) and the International Commission on Non–Ionizing Radiation Protection (ICNIRP) are not related to efficiency but to actual power generated at the receiver side, drive frequency, magnetic flux density, and specific absorption rates (SARs) [12–14]. The average energy flux density and average power density carried by an electromagnetic wave are shown to be proportional to its frequency and frequency squared, respectively [15]. However, the relationship between the power captured by a receiver and the wave frequency, which depends on the physics of energy conversion it obeys, has not been thoroughly studied. Exploring the direct influence of drive frequency on the generated power of a given mechanism could create a convenient bridge for designing an efficient WPTS used for biomedical applications, particularly when subject to safety requirements.

In contrast to WPT, energy harvesting (EH) systems convert the available energy from environmental sources and provide enduring power without any 'cost' [16]. In recent years, inductively scavenging energy from current–carrying structures such as power lines has demonstrated its potential as an approach to power wireless sensor networks [17–19]. Instead of efficiency, the output power (or sometimes the power density) is the paramount quantity of interest for an EH system. Determining the power–frequency dependence in the relationships with other parameters and how this dependence changes under different scenarios (e.g. resonant or non–resonant) could bring further insight into these devices.

In this paper, we investigate both the efficiency and output power of the RIC and ME WPTSs and determine the conditions to maximize these two quantities. The central objectives are to explore the changes in power generation and transfer efficiency under the variations of the drive frequency. RIC WPTS has been largely investigated in the literature. However, here we not only summarize classic, well–known results but also further interpret them and explore the unrevealed properties to form the most comprehensive and universal framework possible for both structures (especially for ME WPTSs). Other efforts are devoted to introducing a figure of merit for each configuration and unifying the expressions of power (and efficiency) of the two architectures in the same general form, written as a function of the figure of merit. Some important results are also applicable to relevant inductive EH or magneto–mechano–electric WPT systems.

There are two possible approaches to determining the relationship between the maximum output power and frequency under the weak coupling assumption. The first option is to decouple the system and only consider the transmitter as a source of magnetic fields. The second choice is to analyze a complete system that includes the dynamics of the transmitter and receiver, then apply the weak–coupled condition to investigate the dependence of power on frequency. We aim to prove that both methods yield the same conclusion. The same point of view is taken for both RIC and ME WPTSs.

2. Power optimization of WPT at weak coupling regime and inductive EH

Figure 1 depicts the key concepts of the inductive-based WPT and EH systems. With the focus on biomedical wearable and implantable applications, in the following study, we presume that the coupling between the transmitter and receiver of the WPTS is weak due to the mismatch between their sizes and a long transfer distance compared to the receiver dimensions. Therefore, the impedance reflected onto either of them is also neglected. The transmitter is now considered a source of magnetic waves that can provide any field strength at any frequency. This analysis, therefore, applies to both EH systems that scavenge energy from magnetic fields available in the environment and weakly–coupled WPTSs.

For a given magnetic flux density $\mathbf{B}$, the magnetic flux passing through a surface $\mathbf{S}$ is

$$\begin{aligned}\Phi &= \iint_S \mathbf{B}\cdot \mathrm{d}\mathbf{S} \\ &= \mathbf{B}\cdot\mathbf{S} = BS\cos\theta \end{aligned} \tag{1}$$

where B is the magnitude of the magnetic flux density, S is the surface area, and θ is the angle between the magnetic field lines and the normal (perpendicular) to $\mathbf{S}$. For the sake of simplification, from now on we consider $\theta = 0$ unless otherwise stated; equivalently, $\Phi = BS$.

Considering a solenoid coil of N turns exposed to a uniform magnetic flux density $\mathbf{B}$ as illustrated in a close-up view of figure 1, according to Faraday's law of induction, the induced electromotive force (EMF) is

$$V_{\mathrm{EMF}} = -N\frac{\mathrm{d}\Phi}{\mathrm{d}t} = -NS\frac{\mathrm{d}B}{\mathrm{d}t}. \tag{2}$$

With a time harmonic magnetic flux density $B(t) = -B_0\sin\omega t$ of angular frequency ω, the EMF can be written as $V_{\mathrm{EMF}} = V_0\cos\omega t$ where

$$V_0 = \omega B_0 NS. \tag{3}$$

Given receiver geometry, V_0 is proportional to ω. When a planar spiral coil is used, $V_0 = \omega B_0\sum_{i=1}^{N} S_{\mathrm{i}}$ where S_{i} is the corresponding area of the ith turn.

When connecting the two terminals of the receiver (or harvester) with an electrical load, the EMF becomes a voltage source of the circuit. The power induced in the load then depends on the magnitude and frequency of the magnetic fields and the impedance characteristics of the receiving system. The primary aim of this section is to explore the relationships between the maximum generated power and the frequency under different scenarios that can take place in practice.

2.1. A general model for small-scale receiver coil

We first investigate the maximum possible power that a receiver or harvester can provide by considering a single-coil resonator loaded with a resistance. A general model of this

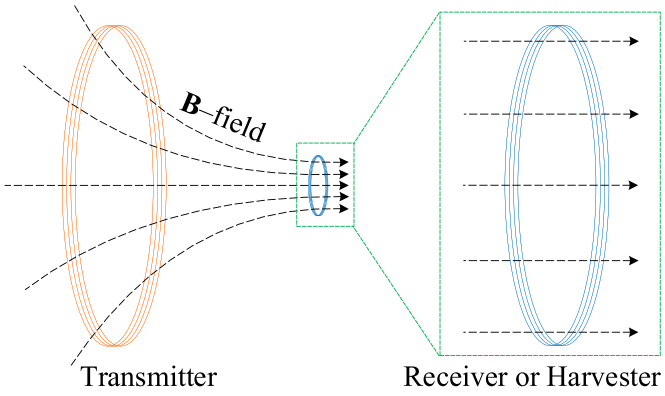

Figure 1. Concepts of a weakly-coupled WPTS and an inductive energy harvester.

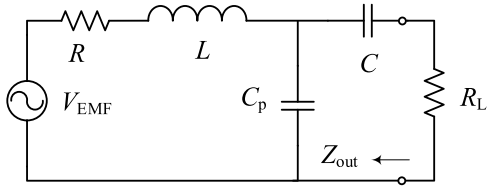

Figure 2. A general model of a coil resonator as a magnetic energy harvester or receiver.

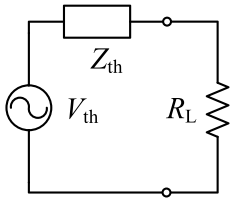

Figure 3. Thévenin equivalent circuit.

resonator is shown in figure 2, in which an external capacitance C is in series with the coil inductance L. In many cases, the coil parasitic capacitance C_p is relatively smaller than C and is neglected. However, C_p may have a significant impact on the dynamics of the receiver and the performance of the output power in principle [20]. Therefore, it is included for a comprehensive analysis.

A convenient method to examine the output power is to use the Thévenin equivalent circuit such as that demonstrated in figure 3. The Thévenin voltage and impedance are derived as follows,

$$V_{th} = V_0 \frac{1/j\omega C_p}{R + j\omega L + 1/j\omega C_p}, \tag{4}$$

$$Z_{th} = Z_{out} = \frac{1}{j\omega C} + \frac{1}{j\omega C_p} \frac{R + j\omega L}{R + j\omega L + 1/j\omega C_p}. \tag{5}$$

The voltage across the load resistance and the output power are given by

$$V_L = \frac{V_{th}}{Z_{out} + R_L} R_L, \tag{6}$$

$$P = \frac{1}{2}\frac{|V_L|^2}{R_L} = \frac{1}{2}\frac{|V_{th}|^2}{|Z_{out} + R_L|^2} R_L. \tag{7}$$

The impedance matching conditions to achieve the maximum power delivered to the load are

$$\begin{cases} \Re\{Z_{out}\} = R_L \\ \Im\{Z_{out}\} = 0, \end{cases} \tag{8}$$

which yield the optimal values of the load resistance and series capacitance as

$$R_L = \frac{R}{(QQ_p - 1)^2 + Q_p^2}, \tag{9}$$

$$C = C_p \frac{(QQ_p - 1)^2 + Q_p^2}{Q_p\big(Q - Q_p(Q^2 + 1)\big)} \tag{10}$$

where $Q = \omega L/R$ and $Q_p = \omega C_p R$. The necessary and sufficient condition such that $C > 0$ is $Q_p < Q/(Q^2 + 1) \leqslant 1/2$. This solution leads to the output power

$$P = \frac{1}{8}\frac{V_0^2}{R} = \frac{1}{8}\frac{(\omega B_0 NS)^2}{R}, \tag{11}$$

which is also the largest possible power the receiver can produce. This maximum power is referred to as the power limit, denoted as P_{lim}.

From the circuit theory point of view, V_{EMF} and R play a role as an effective power source for a lossless two-port network formed by $\{L, C_p, C\}$, and P_{lim} is the power available for extraction. In the later stage, the output port of the T–network is connected to the load resistance R_L at which the electrical energy converted is consumed. Equation (11) is a simple and efficient means to predict the maximum output power of a magnetic energy harvester (also known as inductive energy harvester, a type of generator that can convert time–varying magnetic fields into electricity) or a weakly coupled WPTS. Especially in the latter case, there is no need to explicitly identify the dynamics of the transmitter, the actual coupling coefficient between the two coils, or the system efficiency, but only the field strength at the receiver. The wave frequency is typically known ahead of time.

The results obtained in this section hold regardless of whether R is a constant or frequency-dependent. It is important to note that the power expression (11) can be considered as a quadratic function of the frequency of the propagating waves when R is nearly unchanged with respect to frequency. In the next sections, we study the relationships between the maximum output power and the frequency under different scenarios in practice where (11) may or may not be reached.

2.2. Case I: low–frequency nonresonant transducer

Magnetic EH systems with a pickup coil usually operate at low frequencies (several tens of Hz to a few kHz), at which the reactance of the parasitic capacitance C_p is much higher than the impedance of the coil and can be considered an open circuit. Therefore, C_p is disregarded. Furthermore, the required

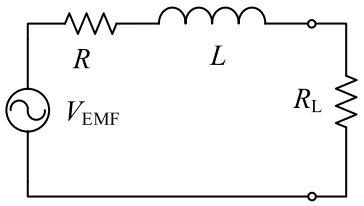

Figure 4. Simplified model for low frequency operation.

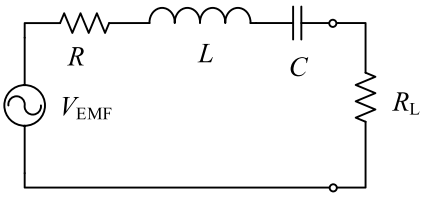

Figure 5. Simplified model for intermediate frequency operation.

optimal capacitance C for forming a resonator is too large to implement. In these circumstances, the general model shown in figure 2 can be simplified to that in figure 4.

The output power now reads as

$$P = \frac{1}{2} V_0^2 \frac{R_L}{(R+R_L)^2 + (\omega L)^2}. \tag{12}$$

Since the two conditions in (8) cannot be satisfied simultaneously, the impedance matching condition is then given by $R_L = |Z_{out}|$ where $Z_{out} = R + j\omega L$. In particular, the optimal load and the corresponding maximum power are

$$R_L = R\sqrt{1+Q^2}, \tag{13}$$

$$P = \frac{1}{8}\frac{V_0^2}{R}\frac{2}{1+\sqrt{1+Q^2}} < P_{lim} = \frac{1}{8}\frac{V_0^2}{R} \forall Q. \tag{14}$$

We note that using the gradient descent method leads to the same results. At low frequency, L and R are almost constant, $V_0^2 \propto \omega^2$ and $Q \propto \omega$. Therefore, $P \propto \omega$ when $Q \gg 1$, approximately.

2.3. Case II: resonant energy harvester and WPT receiver

We now consider a scenario where C_p is still negligibly small and is ignored. However, at the same time, there exists suitable capacitance C connected in series with L to form a resonator. This configuration is described in figure 5, in which the operating frequency is usually between a few tens kHz up to a few tens MHz.

The generated power in this case is computed as

$$P = \frac{1}{2} V_0^2 \frac{R_L}{(R+R_L)^2 + (\omega L - 1/\omega C)^2}. \tag{15}$$

Similarly, the optimal values of load resistance and output power are

$$R_L = R\sqrt{1+(Q-1/Q_c)^2}, \tag{16}$$

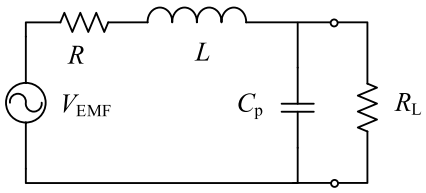

Figure 6. Simplified model for high frequency range.

$$P = \frac{1}{8}\frac{V_0^2}{R}\frac{2}{1+\sqrt{1+(Q-1/Q_c)^2}} \leqslant P_{lim} \forall \{Q, Q_c\} \tag{17}$$

where $Q_c = \omega RC$. At the resonance frequency $\omega_0 = 1/\sqrt{LC}$, we have $QQ_c = 1$, $R_L = R$, and the equality is attained.

In brief, in order to maximize the output power, the resonance frequency ω_0 of the resonator needs to be tuned to match the magnetic field frequency ω, and the load resistance is adapted to the resistance of the coil simultaneously. Similar to (11), $P \propto \omega^2$.

2.4. Case III: high–frequency WPT receiver

For a WPTS operating at high frequencies (sub–MHz and above), the effect of the parasitic capacitance is significant and must be taken into account. On the contrary, the use of an external capacitor may no longer be feasible. And more importantly, it may be not necessary. The following analysis is to clarify this argument.

The equivalent circuit for this circumstance is shown in figure 6. The power delivered to the load is determined by

$$\begin{aligned} P &= \frac{1}{2} V_0^2 \frac{R_L}{|R_L + (j\omega R_L C_p + 1)(R + j\omega L)|^2} \\ &= \frac{1}{2}\frac{V_0^2}{R_L}\frac{1}{[1+R/R_L - QQ_p]^2 + [QR/R_L + Q_p]^2}. \end{aligned} \tag{18}$$

Using the gradient descent approach, the optimal load at each frequency is

$$R_L = R\sqrt{\frac{1+Q^2}{(1-QQ_p)^2 + Q_p^2}}. \tag{19}$$

Moreover, the optimal load and frequency can be simultaneously determined by the impedance matching conditions $\Re\{Z_{out}\} = R_L$ and $\Im\{Z_{out}\} = 0$ where

$$Z_{out} = \frac{1}{j\omega C_p}\frac{R + j\omega L}{R + j\omega L + 1/j\omega C_p}, \tag{20}$$

which results in the solution

$$R_L = R(1+Q^2), \tag{21}$$

$$\omega^2 = (LC_p)^{-1} - (R/L)^2. \tag{22}$$

This solution is real for $L > C_p R^2$, or equivalently, $Q > Q_p$. Note that (21) is a particular case of (19) at a specific frequency ω that is given by (22). From (21) and (22), we observe

that both optimal frequency and load resistance solely depend on the electrical characteristics of the coil $\{L, R, C_p\}$. We also have the relation $1/Q_p = Q + 1/Q$.

At the optimal load and frequency conditions, the corresponding maximum output power is

$$P = \frac{1}{8}\frac{V_0^2}{R} = P_{lim}. \tag{23}$$

This result shows that P is still able to reach its global maximum P_{lim} without the need for an added capacitance. In practice where the wave frequency is known beforehand, it is desired to design a receiver coil whose properties satisfy the condition (22), and the load resistance is chosen based on (21).

The results obtained in this subsection are applicable for a receiver resonator configured in parallel, in which C_p now represents the sum of the added capacitance and the parasitic capacitance. Given the same resonator parameters, the optimal frequency of the parallel configuration is slightly smaller than that of the series structure. Meanwhile, the optimal load resistance of the former is higher than that of the latter. Therefore, choosing which type of connection, series or parallel, strongly depends on the loading condition.

The findings presented in three cases {I, II, III} together with a more general form shown in figure 2 can cover the most commonly used structures in EH and WPT systems. These investigations provide explicit relationships between the maximum output power and operating frequency, and at the same time, show how to reach the power limits under each circumstance.

2.5. On the constant magnetic field

Considering the weak coupling condition in which the reflected impedance on the transmit side of a RIC WPTS is negligible, the generated magnetic field then solely depends on the transmitter geometry and the current flowing in it. A constant current amplitude that produces a constant **B**–field can be accomplished by adapting an external series-capacitance such that the imaginary parts of the transmitter impedance cancel out each other, which is equivalent to forming a resonator. Under the resonance condition, the input current is a function of the coil resistance, but not inductance, and therefore is independent of frequency. This technique is able to produce constant magnetic field strength over a wide range of frequencies.

3. Efficiency consideration of a RIC WPTS

When the transfer efficiency is chosen as the objective of the study, the output power is bounded by the power available from a source. For a given power source, the magnetic field strength is determined by the current flowing into the transmitter coil, which depends on the input impedance of the system that is a function of the operating frequency. Therefore, B_0 is not independent of ω in general. This is the fundamental difference between the efficiency maximization and power optimization problems presented in section 2. The efficiency is obviously always less than unity. However, the dependence of the efficiency on the drive frequency is still of great interest.

The maximum achievable transfer efficiency for a two-coil RIC WPTS is asymptotically expressed in the following form [21, 22]

$$\eta = \frac{k^2 Q_1 Q_2}{\left(\sqrt{1 + k^2 Q_1 Q_2} + 1\right)^2} \tag{24}$$

where Q_1 and Q_2 are the unloaded quality factors of the transmitter and receiver coils, respectively. In particular, $Q_i = \omega L_i / R_i$, where $i = \{1, 2\}$. The coupling coefficient is defined by $k = M/\sqrt{L_1 L_2}$, where M is the mutual inductance between the two coils. L_i and R_i are the inductance and resistance of coil i. The efficiency expression (24) is applicable to approximate the global optimum efficiency of the four configurations, series–series, series–parallel, parallel–series, and parallel–parallel [22]. It is essential to note that (24) is attained if and only if the impedance matching conditions to both source and load are satisfied, that is

$$\begin{cases} R_s = R_1\sqrt{1 + k^2 Q_1 Q_2}, \\ R_L = R_2\sqrt{1 + k^2 Q_1 Q_2}, \end{cases} \tag{25}$$

and $\omega = 1/\sqrt{L_i C_i}$. The corresponding maximum output power is

$$P = \eta P_{avs}. \tag{26}$$

Here, $P_{avs} = |V_s|^2/8R_s$ is the power available from the source that is represented by a series circuit with a source voltage V_s and a resistor R_s. For a given power source, P_{avs} is defined and independent of frequency. It is apparent that P is a linear function of η in the form of $y = ax$.

Some authors refer the term $k^2 Q_1 Q_2$ to as the figure of merit of a RIC WPTS since it directly determines the magnitude of the transfer efficiency. An obvious observation is that η always increases with the increase of $k^2 Q_1 Q_2$. Given the geometries of the transmitter and receiver and the distance between them, the coupling coefficient is a constant. A convenient approach to enhance $k^2 Q_1 Q_2$ is to enlarge the Q–factors by operating at higher frequencies.

In the weak coupling regime, $k^2 Q_1 Q_2 \ll 1$, the optimal load (i.e. the second condition in (25)) is approximately $R_L \approx R_2$. This result coincides with that in section 2.3, which indicates that *maximizing the efficiency is considered equivalent to optimizing the output power under a given magnetic field for the weakly coupled condition*. At the same time, matching the source resistance with that of the transmitter coil $R_s \approx R_1$ maximizes the input power, and as a consequence, the **B**–field generated. The maximum efficiency and output power can be approximated by

$$\eta \approx \frac{1}{4} k^2 Q_1 Q_2, \tag{27}$$

$$P \approx \frac{P_{avs}}{4} k^2 Q_1 Q_2. \tag{28}$$

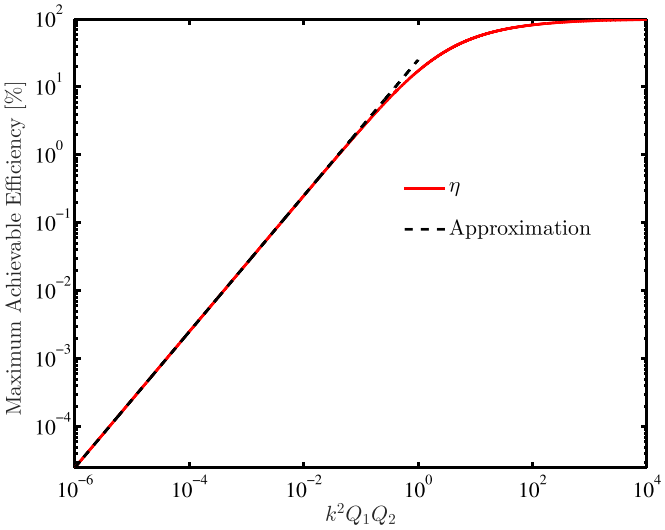

Figure 7. Maximum achievable transfer efficiency in percentage of a RIC WPTS with respect to a figure of merit $k^2Q_1Q_2$.

A comparison between the maximum achievable efficiency and its estimation at weak coupling is shown in figure 7. Under the situation where $k^2Q_1Q_2 \ll 1$, both η and P are proportional to frequency squared since $Q_1Q_2 \propto \omega^2$.

It should be emphasized that, in the low coupling regime, no matter whether we neglect the reflected impedances on the transmitter and receiver sides or we consider the dynamics of the entire system, the quadratic relationship between the maximum output power and the frequency always holds. However, the derivations in section 2.1 are favorable to approximate P since determining the **B**–field strength generated by the transmitter at the receiver location is more convenient than measuring the coupling between the two coils. For a strongly coupled RIC WPTS with high quality factors, $k^2Q_1Q_2 \gg 1$, $\eta \approx 1 - 2/\sqrt{x} + 2/x \to 1$ and $P \to P_{\text{avs}}$, where x represents $k^2Q_1Q_2$.

4. Power optimization of ME WPT and EH

The concept of a ME WPTS is depicted in figure 8, in which the transmitter is a circular coil similar to that of a RIC WPTS, but the receiver in this case is a ME transducer composed of two magnetostrictive layers and one piezoelectric layer instead of a pick-up coil. The magnetic energy captured by the magnetostrictive material is transformed into the vibration of the ME composite. The vibrational kinetic energy is then converted to electricity through the direct piezoelectric effect.

It is possible to operate a RIC WPTS at different frequency bands *with given geometries of the two coils* by choosing appropriately external capacitances. However, the optimum operating frequency of a ME WPTS is usually at or near the mechanical resonance or anti-resonance frequencies. These two specific frequencies are directly dependent on the receiver geometry. Therefore, geometry optimization and the power–frequency relationship are always two inseparable problems

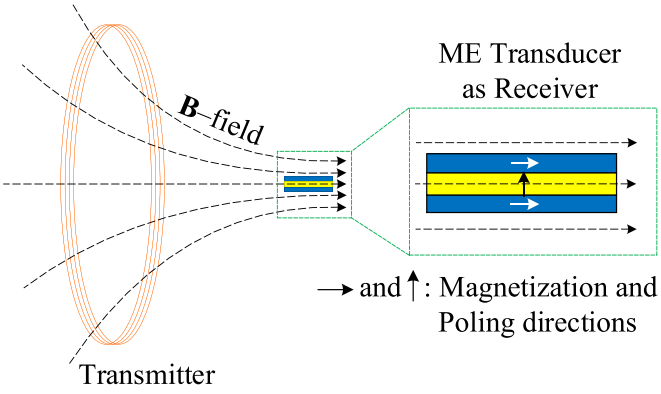

Figure 8. Concept of a ME-based WPTS.

for a ME WPTS. A thorough study to address the relevant questions was presented in [23].

Mechanical Q–factor, a dimensionless parameter, is widely used as a criterion to examine the efficiency of a mechanical system [24]. In order to evaluate the performance of a ME WPTS as fairly as possible when subject to the change of the receiver geometric dimensions, we assume that the mechanical quality factor is constant and is independent of the geometry. Following this assumption, it is shown that the maximum output power is proportional to the operating frequency [23]. More importantly, such a property holds regardless of the magnitude of the volume constraint.

5. Efficiency and figures of merit of a ME WPT

Figure 9 shows an equivalent circuit model to investigate the overall transfer efficiency of a ME WPTS. The internal impedance of the source is expressed in a general form of $Z_{\text{s}} = R_{\text{s}} + jX_{\text{s}}$. L_1 and R_1 represent the inductance and resistance of the transmitter coil, and C_1 is an external capacitor connected in series with $\{L_1, R_1\}$. Ψ_{m} is the effective electrodynamic transduction factor that relates the input current and the electromotive voltage V_{e} to the equivalent force F_0 acting on the ME composite and its longitudinal velocity respectively. Z denotes the mechanical impedance, and b is the mechanical damping coefficient. The coupling between the mechanical and electrical domains at the final stage of the conversion is represented by the electromechanical transduction factor Γ_{p}. C_0 is the nominal capacitance of the piezoelectric element (parasitic capacitances are typically very small by comparison to the piezoelectric capacitance), and R_{L} is the load resistance connected at the output terminals of the ME transducer.

Two widely used criteria to evaluate the performance of a two-port network are the transducer power gain η_{t} and the operating power gain η_{p}, defined as

$$\eta_{\text{t}} = \frac{\text{power delivered to the load}}{\text{power available from the source}} = \frac{P_{\text{L}}}{P_{\text{avs}}}, \tag{29}$$

$$\eta_{\text{p}} = \frac{\text{power delivered to the load}}{\text{power input to the network}} = \frac{P_{\text{L}}}{P_{\text{in}}}, \tag{30}$$

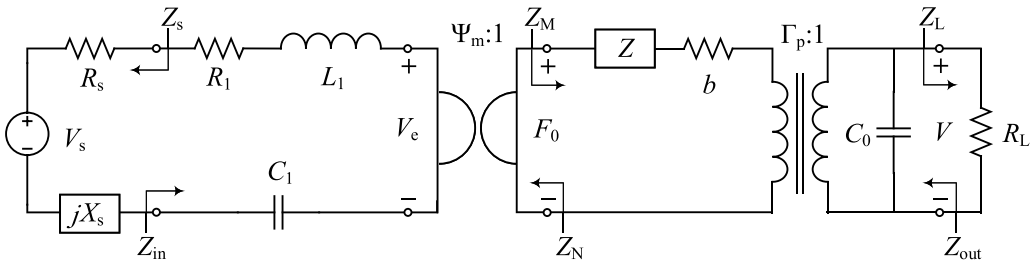

Figure 9. A complete model of a ME WPTS.

in which η_p is usually referred to as the power transfer efficiency or the link efficiency in the field of WPT. η_t is a lower bound of η_p since $\eta_t \leqslant \eta_p$ for any WPTS. We now maximize η_t and η_p based on impedance matching principle. We choose R_s, X_s, C_1, ω and R_L, which are not characteristics of the transmitter or receiver, as objective variables of the optimization problem.

Ψ_m, Z, Γ_p and C_0 are derived as

$$\Psi_m = \Lambda_{H-I}\Gamma_m = \Lambda_{H-I}(2wt_m d_{33,m}/s_{33}^H), \tag{31}$$

$$Z = -j\left(\frac{n}{s_{11}^E} + \frac{1-n}{\kappa s_{33}^H}\right)\frac{A}{2\overline{v}}\cot\frac{\omega L}{2\overline{v}}, \tag{32}$$

$$\Gamma_p = -wd_{31,p}/s_{11}^E, \tag{33}$$

$$C_0 = \epsilon_{33}^S wL/t_p. \tag{34}$$

Λ_{H-I} is a coefficient describing the relationship between the current input to the transmitter coil and the magnetic field strength it generates at the location of the ME device. Λ_{H-I} is dependent on the coil geometry, distance between transmitter and ME device, and the orientation of the ME device relative to the transmit coil. An example of how to determine Λ_{H-I} for a thick coil with rectangular cross section is presented in appendix A. Γ_m is the magneto-elastic transduction factor (it is also sometimes referred to as the electrodynamic transduction factor). The definitions of the material constants and other necessary quantities are as follows. L and w are the length and width of the ME laminate, while t_p and t_m are the thicknesses of the piezoelectric and magnetostrictive layers, respectively. $d_{33,m}$—the piezomagnetic constant. s_{33}^H—the elastic compliance at constant magnetic field. s_{11}^E—elastic compliance of the piezoelectric material under constant electric field. $d_{31,p}$—transverse piezoelectric charge constant. ϵ_{33}^T—dielectric permittivity under constant stress. ϵ_{33}^S—permittivity component at constant strain with the plane-stress assumption of a thin narrow beam (i.e. $\epsilon_{33}^S = \epsilon_{33}^T - d_{31,p}^2/s_{11}^E$). κ is the interface coupling coefficient relating the stress transferred between the magnetostrictive and piezoelectric materials, $0 \leqslant \kappa \leqslant 1$. A, n and $\overline{v}^2$ are the cross-sectional area, the thickness ratio, and the squared speed of sound in the composite, respectively,

$$A = w(t_p + 2t_m), \tag{35}$$

$$n = t_p/(t_p + 2t_m), \tag{36}$$

$$\begin{aligned}\overline{v}^2 &= \frac{1}{\overline{\rho}}\left[n\left(s_{11}^E - \frac{d_{31,p}^2}{\epsilon_{33}^T}\right)^{-1} + \frac{1-n}{\kappa}\left(s_{33}^H - \frac{d_{33,m}^2}{\mu_{33,m}^T}\right)^{-1}\right] \\ &= \left[n/s_{11}^D + (1-n)/\left(\kappa s_{33}^B\right)\right]/\overline{\rho},\end{aligned} \tag{37}$$

$\mu_{33,m}^T$ is the magnetic permeability at constant stress. The equivalent mass density of the ME laminate is

$$\overline{\rho} = n\rho_p + (1-n)\rho_m/\kappa \tag{38}$$

where ρ_p and ρ_m are the mass densities of the piezoelectric and magnetostrictive materials, respectively.

Writing Z in the form of $Z = jZ_0$, the input and output impedances are

$$Z_{in} = j\omega L_1 + \frac{1}{j\omega C_1} + \frac{\Psi_m^2}{Z_M} + R_L, \tag{39}$$

$$Z_{out} = \frac{\dfrac{1}{j\omega C_0}\dfrac{jZ_0 + Z_N + b}{\Gamma_p^2}}{\dfrac{1}{j\omega C_0} + \dfrac{jZ_0 + Z_N + b}{\Gamma_p^2}} \tag{40}$$

where the intermediate parameters Z_M and Z_N are

$$\begin{aligned}Z_M &= Z + b + \Gamma_p^2\frac{R_L}{1 + j\omega R_L C_0} \\ &= jZ_0 + b + \Delta K_p\frac{\tau_p}{1 + j\omega\tau_p},\end{aligned} \tag{41}$$

$$Z_N = \frac{\Psi_m^2}{j\omega L_1 + \dfrac{1}{j\omega C_1} + R_1 + R_s + jX_s}, \tag{42}$$

with $\Delta K_p = \Gamma_p^2/C_0$ and $\tau_p = R_L C_0$.

In order to form a resonator at the transmitter side, C_1 is determined by the relation $j\omega L_1 + (j\omega C_1)^{-1} = 0$, which results in

$$C_1 = (\omega^2 L_1)^{-1}, \tag{43}$$

then $Z_{in} = R_1 + \Psi_m^2/Z_M$. From (41), we have

$$\Re\{Z_M\} = b + \Delta K_p\frac{\tau_p}{1 + (\omega\tau_p)^2}, \tag{44}$$

$$\Im\{Z_{\mathrm{M}}\} = Z_0 - \Delta K_{\mathrm{p}} \frac{\omega\tau_{\mathrm{p}}^2}{1+(\omega\tau_{\mathrm{p}})^2}. \tag{45}$$

Let us choose the operating frequency such that

$$\Im\{Z_{\mathrm{M}}\} = 0, \tag{46}$$

the real and imaginary parts of the input impedance become

$$\Re\{Z_{\mathrm{in}}\} = R_1 + \frac{\Psi_{\mathrm{m}}^2}{b + \Delta K_{\mathrm{p}}\tau_{\mathrm{p}}(1+(\omega\tau_{\mathrm{p}})^2)^{-1}}, \tag{47}$$

$$\Im\{Z_{\mathrm{in}}\} = 0. \tag{48}$$

The conditions for matching to the source impedance are

$$R_{\mathrm{s}} = \Re\{Z_{\mathrm{in}}\}, \tag{49}$$

$$X_{\mathrm{s}} = -\Im\{Z_{\mathrm{in}}\} = 0. \tag{50}$$

Under these circumstances, the input power is equal to the power available from the source, $P_{\mathrm{in}} = P_{\mathrm{avs}}$. Therefore, the two power gains collapse to the same solution, $\eta_{\mathrm{t}} = \eta_{\mathrm{p}} = \eta$. In addition, due to (50), the power available from the source takes the form $P_{\mathrm{avs}} = |V_{\mathrm{s}}|^2/(8R_{\mathrm{s}})$.

The power delivered to the load is given by [23]

$$P = \frac{1}{2}\Delta K_{\mathrm{p}} \frac{\omega^2\tau_{\mathrm{p}}}{1+(\omega\tau_{\mathrm{p}})^2} F_0^2 \Bigg/ \left\{ \left[\overline{Z} + \Delta K_{\mathrm{p}} \frac{(\omega\tau_{\mathrm{p}})^2}{1+(\omega\tau_{\mathrm{p}})^2}\right]^2 + \left[\omega b + \Delta K_{\mathrm{p}} \frac{\omega\tau_{\mathrm{p}}}{1+(\omega\tau_{\mathrm{p}})^2}\right]^2 \right\} \tag{51}$$

where $\overline{Z} = j\omega Z = -\omega Z_0$, and the equivalent force is computed as

$$F_0 = \frac{\Psi_{\mathrm{m}}|V_{\mathrm{s}}|}{\sqrt{(R_{\mathrm{s}} + \Re\{Z_{\mathrm{in}}\})^2 + (\Im\{Z_{\mathrm{in}}\})^2}} = \frac{\Psi_{\mathrm{m}}|V_{\mathrm{s}}|}{2R_{\mathrm{s}}}. \tag{52}$$

We can write

$$\begin{aligned} \overline{Z} + \Delta K_{\mathrm{p}} \frac{(\omega\tau_{\mathrm{p}})^2}{1+(\omega\tau_{\mathrm{p}})^2} &= -\omega \left[Z_0 - \Delta K_{\mathrm{p}} \frac{\omega\tau_{\mathrm{p}}^2}{1+(\omega\tau_{\mathrm{p}})^2} \right] \\ &= -\omega\Im\{Z_{\mathrm{M}}\} = 0, \end{aligned} \tag{53}$$

due to the equality in (46). From (51), (52), and (53), the power transfer efficiency reads

$$\begin{aligned} \eta &= \Delta K_{\mathrm{p}} \frac{\omega^2\tau_{\mathrm{p}}}{1+(\omega\tau_{\mathrm{p}})^2} \frac{\Psi_{\mathrm{m}}^2}{R_{\mathrm{s}}} \left[\omega b + \Delta K_{\mathrm{p}} \frac{\omega\tau_{\mathrm{p}}}{1+(\omega\tau_{\mathrm{p}})^2}\right]^{-2} \\ &= \frac{\Delta K_{\mathrm{p}}}{\omega b} \frac{\omega\tau_{\mathrm{p}}}{1+(\omega\tau_{\mathrm{p}})^2} \frac{\Psi_{\mathrm{m}}^2}{bR_{\mathrm{s}}} \left[1 + \frac{\Delta K_{\mathrm{p}}}{\omega b} \frac{\omega\tau_{\mathrm{p}}}{1+(\omega\tau_{\mathrm{p}})^2}\right]^{-2}. \end{aligned} \tag{54}$$

We now consider a condition to match the output impedance Z_{out} to the load, $R_{\mathrm{L}} = |Z_{\mathrm{out}}|$, to further optimize η. From (43) and (50), it follows that

$$Z_{\mathrm{N}} = \frac{\Psi_{\mathrm{m}}^2}{R_1 + R_{\mathrm{s}}} = \Delta K_{\mathrm{m}}\tau_{\mathrm{m}} \tag{55}$$

where we have introduced $\Delta K_{\mathrm{m}} = \Psi_{\mathrm{m}}^2/L_1$ and $\tau_{\mathrm{m}} = L_1/(R_1 + R_{\mathrm{s}})$, which are analogous to the definitions of ΔK_{p} and τ_{p}, respectively. From (40), we have that

$$|Z_{\mathrm{out}}| = \frac{1}{\omega C_0} \frac{\sqrt{(Z_0/b)^2 + (1+Z_{\mathrm{N}}/b)^2}}{\sqrt{(\Delta K_{\mathrm{p}}/(\omega b) - Z_0/b)^2 + (1+Z_{\mathrm{N}}/b)^2}}. \tag{56}$$

Substituting Z_0 obtained from equations (45) and (46) into the fraction Z_0/b, we get

$$\frac{Z_0}{b} = \frac{\Delta K_{\mathrm{p}}}{\omega b} \frac{(\omega\tau_{\mathrm{p}})^2}{1+(\omega\tau_{\mathrm{p}})^2} = M_{\mathrm{p}} \frac{X^2}{1+X^2} \tag{57}$$

where $M_{\mathrm{p}} = \Delta K_{\mathrm{p}}/(\omega b)$ is an electromechanical figure of merit and $X = \omega\tau_{\mathrm{p}} > 0$. In the same manner, we can write $Z_{\mathrm{N}}/b = M_{\mathrm{m}}Q_{\mathrm{t}}$ where $M_{\mathrm{m}} = \Delta K_{\mathrm{m}}/(\omega b)$ and $Q_{\mathrm{t}} = \omega\tau_{\mathrm{m}} = \omega L_1/(R_1 + R_{\mathrm{s}})$. The parameter M_{m} can be considered as an electrodynamic figure of merit. Alternative forms of M_{p} and M_{m} expressed in terms of the coupling coefficients and the mechanical quality factor of the ME transducer, which are widely utilized in EH and WPT literature, are discussed in appendix B. Q_{t} is the effective quality factor of the transmitter coil, which takes both dissipative components R_{s} and R_1 into account. Setting the right hand side of (56) equal to R_{L}, we obtain

$$X = \frac{\sqrt{\left(M_{\mathrm{p}} \frac{X^2}{1+X^2}\right)^2 + (1+M_{\mathrm{m}}Q_{\mathrm{t}})^2}}{\sqrt{\left(M_{\mathrm{p}} - M_{\mathrm{p}} \frac{X^2}{1+X^2}\right)^2 + (1+M_{\mathrm{m}}Q_{\mathrm{t}})^2}}. \tag{58}$$

Denoting $X^2 = Y > 0$, equation (58) can be simplified as follows

$$(1-Y)\left[(1+M_{\mathrm{m}}Q_{\mathrm{t}})^2(1+Y)^2 - M_{\mathrm{p}}^2 Y\right] = 0. \tag{59}$$

One obvious solution from the first factor is $Y = 1$, in other words,

$$\omega\tau_{\mathrm{p}} = 1. \tag{60}$$

In this case, the equation to find ω is

$$2Z_0\omega = \Delta K_{\mathrm{p}}, \tag{61}$$

following (45) and (46); notice that Z_0 is also a function of ω, $Z_0 = Z_0(\omega)$.

The expression (54) now reduces to

$$\begin{aligned} \eta &= \frac{\Psi_{\mathrm{m}}^2}{bR_{\mathrm{s}}} \frac{M_{\mathrm{p}}/2}{(1+M_{\mathrm{p}}/2)^2} = 2\frac{\Psi_{\mathrm{m}}^2}{bR_{\mathrm{s}}} \frac{M_{\mathrm{p}}}{(M_{\mathrm{p}}+2)^2} \\ &= 2M_{\mathrm{m}}Q_{\mathrm{s}} \frac{M_{\mathrm{p}}}{(M_{\mathrm{p}}+2)^2} \end{aligned} \tag{62}$$

where we define $Q_{\mathrm{s}} = \omega\tau_{\mathrm{s}} = \omega L_1/R_{\mathrm{s}}$, a non–dimensional parameter that is analogous to a quality factor. Q_{s} is an intermediate quantity used for further derivations. We note that the

unloaded quality factor of the transmitter coil is characterized by $Q_1 = \omega\tau_1 = \omega L_1/R_1$. Due to the relations given in (47), (49) and (60), the ratio between Q_s and Q_1 can be written as

$$\frac{Q_s}{Q_1} = \frac{R_1}{R_s} = \frac{M_p + 2}{2M_m Q_1 + M_p + 2}. \tag{63}$$

From (62) and (63), η can be described in terms of three variables, the two figures of merit M_m and M_p, and the resonator unloaded quality factor Q_1,

$$\eta = \frac{2M_m Q_1}{2M_m Q_1 + M_p + 2}\frac{M_p}{M_p + 2}. \tag{64}$$

We would like to emphasize that $\{M_m, M_p, Q_1\}$ are solely dependent on the properties of the transmitter and receiver, and the expression (64) is the maximum power transfer efficiency with the optimal load that satisfies condition (60).

The other factor in (59) leads to the solution

$$\frac{Y}{(1+Y)^2} = \frac{(1+M_m Q_t)^2}{M_p^2}, \tag{65}$$

or equivalently,

$$\frac{\omega\tau_p}{1+(\omega\tau_p)^2} = \frac{1+M_m Q_t}{M_p}, \tag{66}$$

which results in

$$\omega\tau_p = \frac{1 \pm \sqrt{1 - \left(2(1+M_m Q_t)/M_p\right)^2}}{2(1+M_m Q_t)/M_p}. \tag{67}$$

This solution is real (and also positive) only if $M_p \geqslant 2(1 + M_m Q_t)$.

From (66) and (54), we get

$$\eta = M_m Q_s \frac{1+M_m Q_t}{(2+M_m Q_t)^2}. \tag{68}$$

Substituting (66) into (49) yields

$$R_s = R_1 + \frac{\Psi_m^2}{b(2+M_m Q_t)}. \tag{69}$$

The relation between the quality factors Q_t and Q_1 is

$$\frac{Q_t}{Q_1} = \frac{R_1}{R_s + R_1} = \frac{2+M_m Q_t}{4 + 2M_m Q_t + M_m Q_1}, \tag{70}$$

which is equivalent to

$$M_m Q_t^2 + 2Q_t - Q_1 = 0. \tag{71}$$

The positive solution to this quadratic equation is

$$Q_t = \frac{\sqrt{M_m Q_1 + 1} - 1}{M_m}. \tag{72}$$

Therefore, $M_m Q_t + 1 = \sqrt{M_m Q_1 + 1}$ and $(M_m Q_t + 2)^2 = (\sqrt{M_m Q_1 + 1} + 1)^2$. The other is negative and not physical. Following the same procedure, we find that

$$Q_s = \frac{Q_1}{\sqrt{M_m Q_1 + 1}}. \tag{73}$$

Inserting (66), (67), and (72) back into (45) and (46), the operating frequency is then determined by the equation

$$\begin{aligned} 2Z_0\omega &= \Delta K_p \left[1 \pm \sqrt{1 - \left(2(1+M_m Q_t)/M_p\right)^2}\right] \\ &= \Delta K_p \left[1 \pm \sqrt{1 - 4(M_m Q_1 + 1)/M_p^2}\right]. \end{aligned} \tag{74}$$

Finally, we substitute Q_t and Q_s into (68) and obtain

$$\begin{aligned} \eta &= \frac{\sqrt{M_m Q_1 + 1}}{\left(\sqrt{M_m Q_1 + 1} + 1\right)^2}\frac{M_m Q_1}{\sqrt{M_m Q_1 + 1}} \\ &= \frac{M_m Q_1}{\left(\sqrt{M_m Q_1 + 1} + 1\right)^2}. \end{aligned} \tag{75}$$

We note that at the critical value when $M_p = M_p^* = 2(1 + M_m Q_t)$, $\omega\tau_p = 1$ (i.e. see (67)), and the two cases collapse to a single solution. Furthermore, we can write the output impedance in (40) and its imaginary part as

$$Z_{out} = \frac{1}{\omega C_0}\frac{jZ_0/b + (Z_N/b + 1)}{(M_p - Z_0/b) + j(Z_N/b + 1)}, \tag{76}$$

$$\Im\{Z_{out}\} = \frac{1}{\omega C_0}\frac{(Z_0/b)(M_p - Z_0/b) - (Z_N/b + 1)^2}{(M_p - Z_0/b)^2 + (Z_N/b + 1)^2}. \tag{77}$$

With $\omega\tau_p = 1$, based on (61), $Z_0/b = M_p/2$ and $M_p - Z_0/b = M_p/2$. In addition, $Z_N/b = M_m Q_t$. As a consequence, $\Im\{Z_{out}\} = 0$, and the equation $R_L = |Z_{out}|$ is equivalent to $R_L = \Re\{Z_{out}\}$. This result shows that at $M_p = M_p^*$, the bi-conjugate impedance matching conditions

$$\begin{cases} Z_{in} = Z_s^*, \\ Z_{out} = Z_L^* \end{cases} \tag{78}$$

are satisfied. Therefore, the expression (75) is the maximum possible efficiency that can be obtained by the ME WPTS under consideration. More importantly, this global optimum can also be achieved at any $M_p > M_p^*$. The previous solution, i.e. (64), with lower transfer efficiency applies for $M_p < M_p^*$.

We see that the efficiency in (75) is independent of the electromechanical figure of merit M_p and is only a function of the electrodynamic figure of merit M_m and the unloaded quality factor Q_1 of the transmitter. Note, that M_m embeds both the electrodynamic coupling coefficient and the mechanical quality factor of the ME receiver. The independence of efficiency from M_p reflects the fact that when M_p reaches M_p^*, further improvements in the piezoelectric material properties do not result in more power output. The increased damping effect from higher electromechanical coupling (i.e. from the piezoelectric material) would reduce the amount of mechanical power available even though a higher percentage of that

power would be converted to electrical power. Hence, both the output power and efficiency saturate for M_p going beyond M_p^*.

It should be noted that while Ψ_m, Z, Γ_p and C_0 presented at the beginning of this section are for a ME WPTS, the analysis and findings apply to a magneto-mechano-electric (MME) WPTS. This is true for translational [25, 26] and rotational [27] architectures, with their corresponding parameters. In many practical scenarios, the internal impedance of a source $Z_s = R_s + jX_s$ and the electrical load R_L are predetermined. In order to realize the general maximum power transfer theorem in [28], two additional networks (e.g. T—or Π–type) can be used as passive impedance matching circuits at both transmitter and receiver sides. A detailed analysis of the method is out of the scope of this work, but an example can be found in [29].

When the coupling between the transmitter coil and the ME receiver is weak, $M_m Q_t \ll 1$. Thus, the solution (67) is approximately $\omega\tau_p \approx (M_p \pm \sqrt{M_p^2 - 4})/2$ with the condition $M_p \geqslant 2$. This alternative expression of (67) along with (60) form the same complete set of solutions to the power optimization problem for a ME WPTS presented in [23], section III. Therefore, *in the weak coupling regime, the efficiency maximization can be considered equivalent to optimizing the output power under an applied magnetic field*. Moreover, obeying the conditions (43) and (49) (now roughly $R_s \approx R_1$) yields the maximum input power and the largest magnetic field that the transmitter coil can produce (for a given power source). Since the two problems are unified, we can also infer that the relationships between the transfer efficiency and frequency are identical to those of power and frequency obtained from optimizing the geometry of the ME transducer. For instance, under the condition of a constant mechanical quality factor, the efficiency is proportional to the chosen operating frequency, $\eta \propto \omega$. For the circumstances where $M_m Q_t \ll 1$, and correspondingly $M_m Q_1 \ll 1$, the optimum transfer efficiency and output power are

$$\eta \approx \frac{1}{4} M_m Q_1, \tag{79}$$

$$P \approx \frac{P_{avs}}{4} M_m Q_1. \tag{80}$$

Comparing (24) and (75), we see that despite the apparent differences in the energy conversion mechanisms, the optimal transfer efficiency of the two topologies, RIC and ME, essentially share the same form $\eta = \Theta/(\sqrt{1+\Theta}+1)^2$. The quantity Θ can be referred to as the figure of merit and receives different values depending on the WPT structure used. Especially, for weakly coupled systems, the maximum efficiency and output power are reduced to the forms $\eta \approx \Theta/4$ and $P \approx P_{avs}\Theta/4$.

6. Experimental validations: a case study for a weakly coupled RIC system

Equations (24–26) are valuable in showing a comprehensive view of a RIC mechanism. However, they are well–known in the literature and therefore are not necessary to be validated further. Rather than that, we utilize their direct consequences, expressions (27) and (28), as additional support for our interest in identifying the dependence of power on frequency.

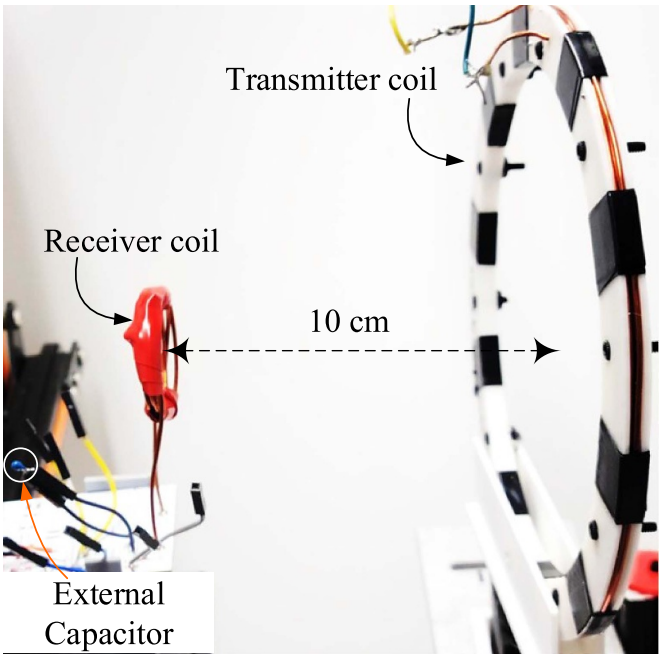

Figure 10. Experimental setup of a weakly–coupled inductive WPTS.

In this section, a RIC WPTS is implemented to experimentally validate a key finding in section 2 that the maximum output power is proportional to the drive frequency squared at the weak coupling regime. The experimental setup is shown in figure 10. The receiver coil is a 3 cm diameter 6–turn solenoid coil composed of 16 AWG (1.291 mm diameter) copper wire. A resonator is formed at the receiving side by connecting an external capacitor in parallel with the receiver coil. This configuration eliminates the effects of the parasitic capacitance (of the receiver), in which the effective capacitance is now a summation of the added capacitance and that parasitic capacitance. The frequency range of interest is within $(0, 250]$ kHz, which is also a typical operating frequency range of a ME WPTS. In this case, the frequency–dependent resistance of the coil (also known as AC resistance) is negligible. Therefore, the coil series resistance can be considered constant and only contains a DC resistance. The transmitter coil is a 15.56 cm diameter 9–turn solenoid coil made of 16 AWG (1.201 mm diameter) copper wire.

The receiver is placed along the centerline of the transmitter and at a distance of 10 cm. The planes of both coils are in parallel (i.e. there is no misalignment). The squared coupling coefficient between the transmitter and receiver of the particular system under investigation is approximately $k^2 \approx 0.01\%$, obtained by COMSOL simulation. Since the coupling is weak, the transmitter coil acts as a pure magnetic field generator. An E&I 240L class A linear power amplifier was used to supply the transmitter coil with a high–frequency current. The **B**–field

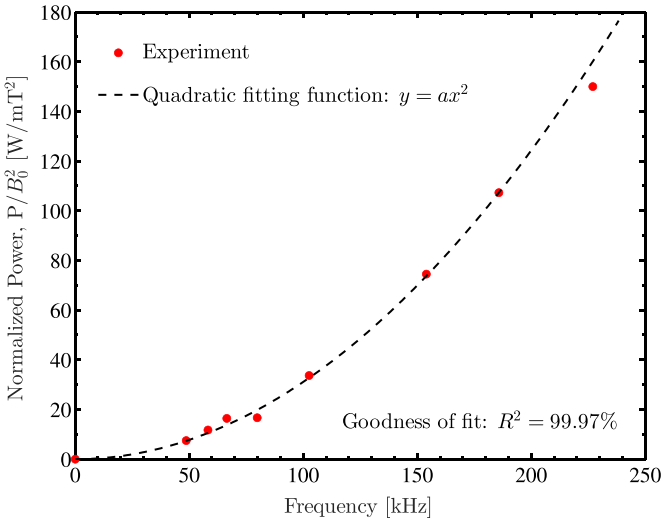

Figure 11. Maximum transferred power with respect to drive frequency, normalized by square of magnetic flux density amplitude.

strength produced at the location of the receiver, B_0, is measured by a MC110A magnetic field sensor (manufactured by Magnetic Sciences Inc.). In order to reduce the complexity of the experimental process, we choose not to form a resonator at the transmitting side and normalize the maximum delivered power with the **B**–field squared instead. As a consequence of (11), this approach does not affect the relationship between output power and frequency, regardless of particular values of B_0. The load resistance is varied to determine its optimal value and the corresponding maximum power at each drive frequency.

Figure 11 shows a comparison between the experimental data and a quadratic approximation of the form $y = ax^2$, where y is the normalized power P/B_0^2 and x is the frequency. We note that B_0 is different at different frequencies in these experiments. The coefficient $a = 3.108 \times 10^{-3}$ is determined by MATLAB Curve Fitting Toolbox. The discrepancy between the measured and fitted quadratic curve is negligible, showing a quadratic dependence of the maximum output power on the drive frequency. This finding is consistent with the theoretical prediction in (11).

Performing experimental validations for a RIC WPTS is straightforward by using different external capacitors to adjust the resonance frequency of a given receiver coil. However, the validation process becomes more complicated for a ME WPTS, which requires many ME composites fabricated with various geometric dimensions to attain different resonance frequencies. Manufacturing multilayer and multi–material ME transducers at a small scale is challenging. Therefore, the experimental study on the power–frequency relationship for ME devices is left open in this work. Since *a complete model taking the dynamics of both the transmitter and receiver has been thoroughly validated by rigorous experiments* [30, 31], the theoretical analysis in sections 4 and 5 is still an appropriate framework for further investigations of other researchers in the field of ME WPT.

7. Discussion

The derivations presented in sections 2 and 3 hold independently of the receiver and harvester structures. However, when the coil geometry is subject to change, the EMF amplitude V_0 and the coil series resistance R become functions of the number of turns N, the drive frequency ω, and the geometric dimensions. In the low—and intermediate–frequency ranges (e.g. up to a few hundreds of kHz), R slightly increases with ω and is approximately proportional to N [32]. Meanwhile, V_0 can be considered proportional to both N and ω. Therefore, P_{lim} (and P) almost always increases with N and ω, assuming that the other parameters such as the magnetic flux density B_0 and the surface area S are kept unchanged. Therefore, increasing the number of turns and the operating frequency is preferable. These characteristics are more important in EH systems that operate at very low frequencies, such as ones that scavenge magnetic energy from a power line [33].

On the other hand, R increases exponentially with ω in higher frequency bands (e.g. sub–MHz). A small change of N may lead to a substantial increase of the overall value of R due to the eddy current and the proximity effect [34–37]. Thus, considering the geometry optimization problem is essential under this scenario, especially when the volume or area is constrained. This concern is out of the scope of the paper and is left open for further study.

The quadratic dependence of the maximum output power and efficiency on the drive frequency observed in sections 2 and 3 is only valid in a frequency range in which the change of the coil series resistance with frequency is small. In order to emphasize this property, without loss of generality, we consider a hypothetical example where two identical spiral coils form a RIC WPTS. The relevant parameters and equations for computing the example are detailed in appendix C. η is obtained using (24) and (27). The variation of inductance with frequency is negligible and usually ignored, while the series resistance of the coil is frequency–dependent, $R = R(\omega)$. The results are presented in figure 12, showing the variation of the coil resistance R in terms of the operating frequency for a given coil geometry and the frequency response of the largest possible transfer efficiency of the considered RIC WPTS. In particular, for $f \leqslant 200$ kHz, R is nearly constant, and therefore, both P and η are proportional to ω^2. However, in a higher frequency range, R increases dramatically and causes a significant decrease in the Q–factors. As a consequence, P and η reduce with frequency after reaching their maximum values at an optimal frequency. For the specific geometry given in appendix C, the optimal frequency is about 1 MHz. This general trend applies to any coil, and the optimal frequency depends on the coil geometry.

The power and efficiency expressions presented in sections 4 and 5 are valid when the demagnetization effects are negligible. For magnetostrictive materials with very high permeability, Metglas for example, the demagnetizing field could significantly decrease both the power and efficiency and thus cannot be ignored [38]. Maximizing transferred power and efficiency associated with the geometry optimization problem

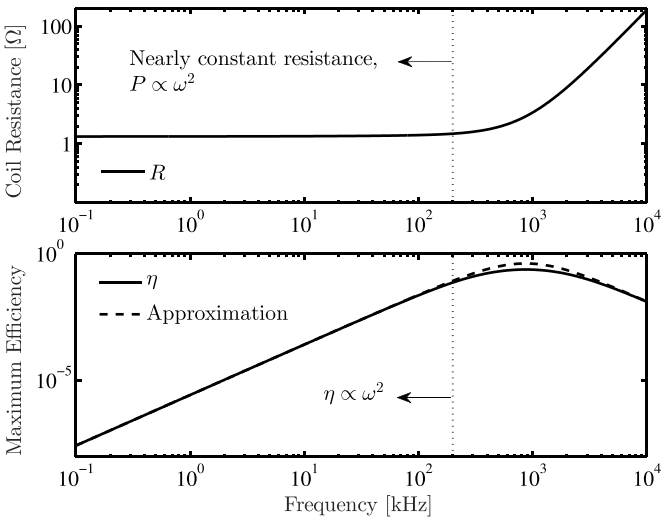

Figure 12. An example of the dependence of the coil series resistance and maximum transfer efficiency on the drive frequency.

becomes much more complicated when taking the demagnetization phenomenon into account. Therefore, using numerical methods to find optimal solutions is more appropriate than analytical counterparts. However, it is essential to note that the presence of the demagnetizing field does not alter the relationship between power/efficiency and frequency, which is still linear with the assumption of a constant mechanical quality factor.

$$\Lambda_{\mathrm{H-I}} = \frac{\mathrm{d}H_0}{\mathrm{d}I} = \frac{1}{4\pi(z_2 - z_1)(r_2 - r_1)} \times \int_{r_1}^{r_2}\int_{\varphi_1}^{\varphi_2}\int_{z_1}^{z_2} \frac{(\widetilde{r} - r\cos\widetilde{\varphi})\widetilde{r}}{(r^2 + \widetilde{r}^2 - 2r\widetilde{r}\cos\widetilde{\varphi} + (z-\widetilde{z})^2)^{3/2}}\mathrm{d}\widetilde{r}\mathrm{d}\widetilde{\varphi}\mathrm{d}\widetilde{z}. \tag{81}$$

Human safety considerations are essential for WPTS used to provide power for biomedical implantable devices, regardless of their energy conversion mechanisms. The International Committee on Electromagnetic Safety (ICES, a subsidiary of IEEE) and ICNIRP have established safety standards for WPTS, especially for exposure to magnetic and electric fields [12–14]. In particular, ICES has regulated dosimetric reference limits (DRLs) for RF shocks (defined in terms of the electric field) and SARs for thermal heating inside the human body. For instance, the limits of the SARs are 0.4 and 10 W kg^{-1} for the whole–body and localized exposures, respectively. Such restrictions are very challenging to measure or predict. Thus, exposure reference levels (ERLs) have been introduced as an alternative. Most of the ERLs are defined as the maximum allowable magnetic flux density with respect to the wave frequency, making them much more convenient to assess. For example, the permissible **B**–field strength at 100 kHz is 100 μT while that at 6.78 MHz is 0.29 μT. Most importantly, the regulations based on ERLs are more conservative than those relied on SARs. In other words, a system complying with the ERLs also simultaneously satisfies the requirements of DRLs and therefore obeys the safety standards [39].

Up to this point, the relationship between a chosen operating frequency and the corresponding ERL, and the relationship between the output power and an applied magnetic field, are relatively well–known. Exploring a direct dependence of power on frequency provides the last bridge connecting the triangle of power–frequency–magnetic field strength. The obtained properties could serve as simple and efficient tools to estimate, design, and optimize the performance of a WPTS, especially when subject to safety restrictions.

8. Conclusion

We discussed four scenarios with two central objectives, maximum output power, and optimum efficiency, for two WPTSs based on RIC and ME effects. We unified the power and efficiency maximization problems for each architecture in the weak coupling regime, in which we found that both schemes yield the same optimal load and frequency. We also resolved the differences in the energy conversion of the two mechanisms by expressing the power and efficiency in similar general forms, respectively. We revealed the quadratic dependence of both quantities (power and efficiency at their maximum) on drive frequency for a RIC system. In the case of a ME configuration, these relationships become linear under a constant mechanical quality factor condition. Although the two considered WPT techniques have been extensively studied in the literature, the findings presented in this paper could provide a more insightful understanding of their performance. In addition, the results can be extended to other relevant systems that share similar physics, such as inductive EH or MME (sometimes referred to as electrodynamic) WPT. Therefore, the angle of view and the approach we chose here could be beneficial to a wide variety range of fields.

Data availability statement

The data that support the findings of this study are available upon reasonable request from the authors.

Appendix A. Current and magnetic field relationship of a thick coil with rectangular cross section

The geometric dimensions of a thick coil that carries an (effective) input current of I are shown in figure 13. The notations are defined as follows. r_1 (r_2)—the inner (outer) radius. z_1 (z_2)—the lower (upper) height. t_c—the total thickness of the coil, usually $z_1 = -z_2 = t_c/2$. For the sake of simplicity, we assume that the ME transducer is in parallel with the centerline of the transmitter coil, hence $H_0 = H_z(r, z)$. The parameter $\Lambda_{\mathrm{H-I}}$ is then given by equation (81) [40], where $\widetilde{r}$, $\widetilde{\varphi}$ and $\widetilde{z}$ are the integration variables, $\varphi_1 = 0$ and $\varphi_2 = 2\pi$. This three-dimensional integral can be numerically computed by the function [*integral3*] in MATLAB. An alternative form of $H_0 = H_z(x, y, z)$ expressed in the Cartesian coordinates can be found in [41].

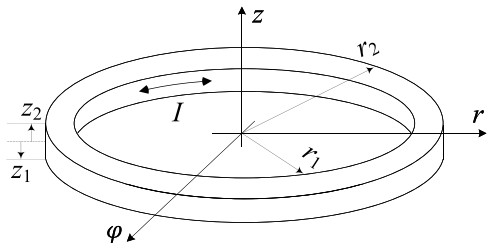

Figure 13. Geometry of a thick coil carrying a uniform current density. Here, I is the effective current flowing in the coil.

Appendix B. Approximations of electromechanical and electrodynamic figures of merit

We first assume that the mechanical impedance Z in (32) can be approximated by a mass–spring systems $\{m, K_0\} > 0$ such that $\omega m - K_0/\omega \approx Z(\omega)$ for all $\omega > 0$. The electrodynamic and electromechanical coupling coefficients are defined by [42, 43]

$$k_{\mathrm{p}}^2 = \frac{\Gamma_{\mathrm{p}}^2}{(\Delta K_{\mathrm{p}} + K_0)C_0} = \frac{\Gamma_{\mathrm{p}}^2}{\Gamma_{\mathrm{p}}^2 + K_0 C_0}, \tag{82}$$

$$k_{\mathrm{m}}^2 = \frac{\Psi_{\mathrm{m}}^2}{(\Delta K_{\mathrm{m}} + K_0)L_1} = \frac{\Psi_{\mathrm{m}}^2}{\Psi_{\mathrm{m}}^2 + K_0 L_1}. \tag{83}$$

The corresponding expedient coupling coefficients [44] (also known as generalized coupling coefficients [45]) are given by

$$k_{\mathrm{p,e}}^2 = \frac{k_{\mathrm{p}}^2}{1 - k_{\mathrm{p}}^2} = \frac{\Gamma_{\mathrm{p}}^2}{K_0 C_0}, \tag{84}$$

$$k_{\mathrm{m,e}}^2 = \frac{k_{\mathrm{m}}^2}{1 - k_{\mathrm{m}}^2} = \frac{\Psi_{\mathrm{m}}^2}{K_0 L_1}. \tag{85}$$

Note that $\{k_{\mathrm{p,e}}^2, k_{\mathrm{m,e}}^2\} \in [0, 1]$ and $\{k_{\mathrm{p,e}}^2, k_{\mathrm{m,e}}^2\} \in [0, \infty)$. The electromechanical and electrodynamic figures of merit can be written

$$M_{\mathrm{p}} = \frac{\Delta K_{\mathrm{p}}}{\omega b} = \frac{\Gamma_{\mathrm{p}}^2}{C_0 \omega b} = k_{\mathrm{p,e}}^2 \frac{m\omega_0^2}{\omega b}, \tag{86}$$

$$M_{\mathrm{m}} = \frac{\Delta K_{\mathrm{m}}}{\omega b} = \frac{\Psi_{\mathrm{m}}^2}{L_1 \omega b} = k_{\mathrm{m,e}}^2 \frac{m\omega_0^2}{\omega b} \tag{87}$$

where $\omega_0 = \sqrt{K_0/m}$ and $K_0 = m\omega_0^2$. Usually, the operating frequency of a ME WPTS is close to the resonance frequency, $\omega \approx \omega_0$. Therefore, M_{p} and M_{m} are approximately

$$M_{\mathrm{p}} \approx k_{\mathrm{p,e}}^2 Q_0, \tag{88}$$

$$M_{\mathrm{m}} \approx k_{\mathrm{m,e}}^2 Q_0 \tag{89}$$

where $Q_0 = \omega m/b$ is the mechanical quality factor of the ME receiver at its resonance frequency.

Appendix C. Spiral coil modeling

While many different types of coil can be used for a WPTS, here we chose a spiral coil structure for the purpose of demonstration since the mathematical model for estimating its electrical properties, such as inductance and series resistance, is quite straightforward. Figure 14 shows the geometry of a spiral coil, in which d_{in} and d are the inner and outer diameters. The copper track thickness, width, and the spacing between two tracks are denoted as t_0, w, and s, respectively.

The equations to compute the coil inductance and total resistance are reported in [4] and summarized as follows.

$$\begin{aligned}
d &= 2(d_{\mathrm{in}}/2 + (n-1)s + nw),\\
\beta &= (d - d_{\mathrm{in}})/(d + d_{\mathrm{in}}),\\
d_{\mathrm{L}} &= (d + d_{\mathrm{in}})/2,\\
L &= \frac{\mu n^2 d_{\mathrm{L}}}{2}\left[\ln\left(\frac{2.46}{\beta}\right) + 0.2\beta^2\right],\\
d_{\mathrm{avg}} &= d - (w+s)n/2,\\
l_{\mathrm{c}} &= \pi d_{\mathrm{avg}} n,\\
A_{\mathrm{c}} &= w t_0,\\
R_{\mathrm{DC}} &= \rho\frac{l_{\mathrm{c}}}{A_{\mathrm{c}}},\\
\delta &= \sqrt{\frac{2\rho}{\omega\mu}},\\
R_{\mathrm{skin}} &= R_{\mathrm{DC}}\frac{t_0}{\delta\left(1 - \exp(-t_0/\delta)\right)}\frac{1}{1 + t_0/w},\\
R_{\mathrm{prox}} &= \frac{R_{\mathrm{DC}}}{10}\left(\frac{\omega}{\omega_{\mathrm{c}}}\right)^2,\\
\omega_{\mathrm{c}} &= \frac{3.1}{\mu_0}\frac{(w+s)\rho}{w^2 t_0},\\
R &= R_{\mathrm{DC}} + R_{\mathrm{skin}} + R_{\mathrm{prox}}.
\end{aligned}$$

For copper conductors, the permeability is approximately $\mu \approx \mu_0$, where $\mu_0 = 4\pi \times 10^{-7}$ NA^{-2} is the permeability of free space. R_{DC} represents the DC loss of the conductor. R_{skin} and R_{prox} are the frequency–dependent components of the resistance due to the skin and proximity effects, respectively. The summation $(R_{\mathrm{skin}} + R_{\mathrm{prox}})$ is also known as AC resistance, instantaneous resistance, or dynamic resistance. β is referred to as the fill–factor. δ is the skin depth. ρ is the resistivity of the material, $\rho = 1.68 \times 10^{-8}$ Ωm for copper at 20 °C. l_{c} and A_{c} are the length and the cross–sectional area of the conductor, respectively. ω_{c} is the critical frequency at which current crowding begins to occur. A RIC WPTS formed by two identical coils is considered, hence $Q_1 = Q_2 = \omega L/R$. The number of turn of each coil is $n = 10$. The coupling coefficient between the transmitter and receiver is arbitrarily chosen as $k^2 = 1\%$. The particular parameter values used are $d_{\mathrm{in}} = 1$ cm, $w = 3$ mm, $s = 2w$ (the inductance of a circular spiral coil is accurately predicted with less than 8 % error for $s \leqslant 3w$), and $t_0 = 35\,\mu$m (for standard plated printed circuit board).

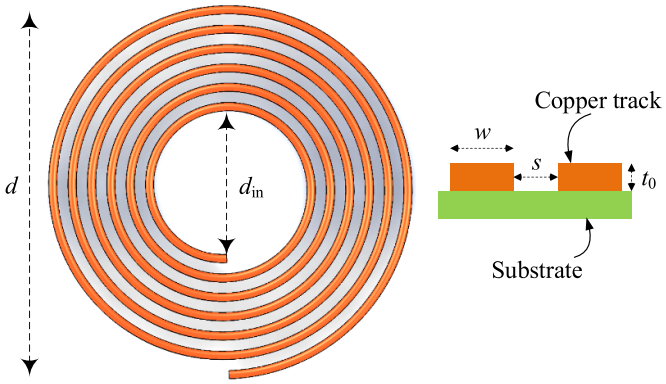

Figure 14. Geometry and parameter definitions of a spiral–shaped coil.

ORCID iD

Binh Duc Truong https://orcid.org/0000-0001-7108-4713

References

[1] Tesla N 1907 Apparatus for transmitting electrical energy *US Patent* US1119732A

[2] Kurs A, Karalis A, Moffatt R, Joannopoulos J D, Fisher P and Soljačić M 2007 Wireless power transfer via strongly coupled magnetic resonances *Science* **317** 83–86

[3] Agarwal K, Jegadeesan R, Guo Y-X and Thakor N V 2017 Wireless power transfer strategies for implantable bioelectronics *IEEE Rev. Biomed. Eng.* **10** 136–61

[4] Schormans M, Valente V and Demosthenous A 2018 Practical inductive link design for biomedical wireless power transfer: a tutorial *IEEE Trans. Biomed. Circuits Syst.* **12** 1112–30

[5] Santis M D and Cacciotti I 2020 Wireless implantable and biodegradable sensors for postsurgery monitoring: current status and future perspectives *Nanotechnology* **31** 252001

[6] Roy S, Azad A N M W, Baidya S, Alam M K and Khan F 2022 Powering solutions for biomedical sensors and implants inside the human body: a comprehensive review on energy harvesting units, energy storage and wireless power transfer techniques *IEEE Trans. Power Electron.* **37** 12237–63

[7] Kim H-J, Hirayama H, Kim S, Han K J, Zhang R and Choi J-W 2017 Review of near-field wireless power and communication for biomedical applications *IEEE Access* **5** 21264–85

[8] Song M, Belov P and Kapitanova P 2017 Wireless power transfer inspired by the modern trends in electromagnetics *Appl. Phys. Rev.* **4** 021102

[9] Nan T *et al* 2017 Acoustically actuated ultra-compact NEMS magnetoelectric antennas *Nat. Commun.* **8** 296

[10] Chen H *et al* 2020 Ultra-compact mechanical antennas *Appl. Phys. Lett.* **117** 170501

[11] Zaeimbashi M *et al* 2021 Ultra-compact dual-band smart NEMS magnetoelectric antennas for simultaneous wireless energy harvesting and magnetic field sensing *Nat. Commun.* **12** 1–11

[12] ICES I 2019 IEEE standard for safety levels with respect to human exposure to electric, magnetic and electromagnetic fields, 0 Hz to 300 GHz *IEEE Std C95.1-2019 (Revision of IEEE Std C95.1-2005/ Incorporates IEEE Std C95.1-2019/Cor 1-2019)* 1–312

[13] International Commission on Non-Ionizing Radiation Protection 2010 Guidelines for limiting exposure to time-varying electric and magnetic fields (1 Hz to 100 kHz) *Health Phys.* **99** 818–36

[14] International Commission on Non-Ionizing Radiation Protection 2020 Guidelines for limiting exposure to electromagnetic fields (100 kHz to 300 GHz) *Health Phys.* **118** 483–524

[15] Muhibbullah M, Haleem A M A and Ikuma Y 2017 Frequency dependent power and energy flux density equations of the electromagnetic wave *Results Phys.* **7** 435–9

[16] Wei C and Jing X 2017 A comprehensive review on vibration energy harvesting: modelling and realization *Renew. Sustain. Energy Rev.* **74** 1–18

[17] Yuan S, Huang Y, Zhou J, Xu Q, Song C and Thompson P 2015 Magnetic field energy harvesting under overhead power lines *IEEE Trans. Power Electron.* **30** 6191–202

[18] Wright S W, Kiziroglou M E, Spasic S, Radosevic N and Yeatman E M 2019 Inductive energy harvesting from current-carrying structures *IEEE Sens. Lett.* **3** 1–4

[19] Kiziroglou M, Wright S and Yeatman E 2020 Coil and core design for inductive energy receivers *Sens. Actuators* A **313** 112206

[20] Truong B D, Roundy C, Andersen E and Roundy S 2019 Analysis of resonance and anti-resonance frequencies in a wireless power transfer system: analytical model and experiments *IEEE Trans. Circuits Syst. II: Express Briefs* **66** 1222–6

[21] Zargham M and Gulak P G 2012 Maximum achievable efficiency in near-field coupled power-transfer systems *IEEE Trans. Biomed. Circuits Syst.* **6** 228–45

[22] Truong B D, Le T T-T and Sensale-Rodriguez B 2020 Two-coil wireless power transfer system configured in series-series topology: fundamental dynamics and limitations on transmitted power (arXiv:2011.14215)

[23] Truong B D 2021 Power optimization of a magnetoelectric wireless power transfer system with volume constraint *Sens. Actuators* A **341** 113226

[24] Erturk A and Inman D 2011 *Piezoelectric Energy Harvesting* (New York: Wiley)

[25] Truong B D and Roundy S 2019 Wireless power transfer system with center-clamped magneto-mechano-electric (MME) receiver: model validation and efficiency investigation *Smart Mater. Struct.* **28** 015004

[26] Challa V R, Mur-Miranda J O and Arnold D P 2012 Wireless power transmission to an electromechanical receiver using low-frequency magnetic fields *Smart Mater. Struct.* **21** 115017

[27] Garraud N, Garraud A, Munzer D, Althar M and Arnold D P 2019 Modeling and experimental analysis of rotating magnet receivers for electrodynamic wireless power transmission *J. Phys. D: Appl. Phys.* **52** 185501

[28] Kong C S 1995 A general maximum power transfer theorem *IEEE Trans. Educ.* **38** 296–8

[29] Truong B D 2019 Investigation on power optimization principles for series-configured resonant coupled wireless power transfer systems *AEU-Int. J. Electron. Commun.* **106** 67–81

[30] Truong B D and Roundy S 2020 Experimentally validated model and power optimization of a magnetoelectric wireless power transfer system in free-free configuration *Smart Mater. Struct.* **29** 085053

[31] Truong B D, Andersen E, Casados C and Roundy S 2020 Magnetoelectric wireless power transfer for biomedical implants: effects of non-uniform magnetic field, alignment and orientation *Sens. Actuators* A **316** 112269

[32] Klaric Felic G, Ng D and Skafidas E 2013 Investigation of frequency-dependent effects in inductive coils for implantable electronics *IEEE Trans. Magn.* **49** 1353–60

[33] Kuang Y, Chew Z J, Ruan T, Lane T, Allen B, Nayar B and Zhu M 2021 Magnetic field energy harvesting from the

traction return current in rail tracks *Appl. Energy* **292** 116911
[34] Dwight H B 1918 Skin effect in tubular and flat conductors *Proc. Am. Inst. Electr. Eng.* **37** 977–98
[35] Cockcroft J D and Rutherford E 1929 Skin effect in rectangular conductors at high frequencies *Proc. R. Soc.* A **122** 533–42
[36] Pantic Z and Lukic S 2013 Computationally-efficient, generalized expressions for the proximity-effect in multi-layer, multi-turn tubular coils for wireless power transfer systems *IEEE Trans. Magn.* **49** 5404–16
[37] Kim J and Park Y-J 2015 Approximate closed-form formula for calculating ohmic resistance in coils of parallel round wires with unequal pitches *IEEE Trans. Ind. Electron.* **62** 3482–9
[38] Aharoni A 1998 Demagnetizing factors for rectangular ferromagnetic prisms *J. Appl. Phys.* **83** 3432–4
[39] Andersen E, Casados C, Truong B D and Roundy S 2021 Optimal transmit coil design for wirelessly powered biomedical implants considering magnetic field safety constraints *IEEE Trans. Electromagn. Compat.* **63** 1735–47
[40] Ravaud R, Lemarquand G, Lemarquand V, Babic S and Akyel C 2010 Calculation of the magnetic field created by a thick coil *J. Electromagn. Waves Appl.* **24** 1405–18
[41] Babic S, Andjelic Z, Krstajic B and Salon S 1988 Analytical calculation of the 3D magnetostatic field of a toroidal conductor with rectangular cross section *IEEE Trans. Magn.* **24** 3162–4
[42] Ikeda T 1996 *Fundamentals of Piezoelectricity* (Oxford: Oxford University Press)
[43] Halvorsen E 2016 Optimal load and stiffness for displacement-constrained vibration energy harvesters (arXiv:1603.01909 [physics.class-ph])
[44] Tadmor E and Kosa G 2003 Electromechanical coupling correction for piezoelectric layered beams *J. Microelectromech. Syst.* **12** 899–906
[45] Renaud M, Elfrink R, Jambunathan M, de Nooijer C, Wang Z, Rovers M, Vullers R and van Schaijk R 2012 Optimum power and efficiency of piezoelectric vibration energy harvesters with sinusoidal and random vibrations *J. Micromech. Microeng.* **22** 105030